

KEK-preprint-94-109
 NWU-HEP 94-05
 TUAT-HEP 94-06
 DPNU-94-41
 TIT-HPE 94-08
 OCU-HEP 94-08
 PU-94-687
 INS-REP-1063
 KOBE-HEP 94-07

Measurement of inclusive electron cross section in $\gamma\gamma$ collisions at TRISTAN *

M.Iwasaki^{(1) †}, R.Enomoto⁽²⁾, H.Hayashii⁽¹⁾, E.Nakano⁽³⁾, K.Abe⁽³⁾, T.Abe⁽³⁾, I.Adachi⁽²⁾, K.Adachi⁽¹⁾, M.Aoki⁽³⁾, M.Aoki⁽⁴⁾, S.Awa⁽¹⁾, K.Emi⁽⁵⁾, H.Fujii⁽²⁾, K.Fujii⁽²⁾, T.Fujii⁽⁶⁾, J.Fujimoto⁽²⁾, K.Fujita⁽⁷⁾, N.Fujiwara⁽¹⁾, B.Howell⁽⁸⁾, N.Iida⁽²⁾, H.Ikeda⁽²⁾, Y.Inoue⁽⁷⁾, R.Itoh⁽²⁾, H.Iwasaki⁽²⁾, R.Kajikawa⁽³⁾, K.Kaneyuki⁽⁴⁾, S.Kato⁽⁹⁾, S.Kawabata⁽²⁾, H.Kichimi⁽²⁾, M.Kobayashi⁽²⁾, D.Koltick⁽⁸⁾, I.Levine⁽⁸⁾, S.Minami⁽⁴⁾, K.Miyabayashi⁽³⁾, A.Miyamoto⁽²⁾, K.Muramatsu⁽¹⁾, K.Nagai⁽¹⁰⁾, K.Nakabayashi⁽³⁾, O.Nitoh⁽⁵⁾, S.Noguchi⁽¹⁾, A.Ochi⁽⁴⁾, F.Ochiai⁽¹¹⁾, N.Ohishi⁽³⁾, Y.Ohnishi⁽³⁾, Y.Ohshima⁽⁴⁾, H.Okuno⁽⁹⁾, T.Okusawa⁽⁷⁾, T.Shinohara⁽⁵⁾, A.Sugiyama⁽³⁾, S.Suzuki⁽³⁾, S.Suzuki⁽⁴⁾, K.Takahashi⁽⁵⁾, T.Takahashi⁽⁷⁾, T.Tanimori⁽⁴⁾, T.Tauchi⁽²⁾, Y.Teramoto⁽⁷⁾, N.Toomi⁽¹⁾, T.Tsukamoto⁽²⁾, T.Tsumura⁽⁵⁾, S.Uno⁽²⁾, T.Watanabe⁽⁴⁾, Y.Watanabe⁽⁴⁾, A.Yamaguchi⁽¹⁾, A.Yamamoto⁽²⁾, and M.Yamauchi⁽²⁾

(TOPAZ Collaboration)

⁽¹⁾ *Department of Physics, Nara Women's University, Nara 630, Japan*

⁽²⁾ *National Laboratory for High Energy Physics, KEK, Ibaraki-ken 305, Japan*

⁽³⁾ *Department of Physics, Nagoya University, Nagoya 464, Japan*

⁽⁴⁾ *Department of Physics, Tokyo Institute of Technology, Tokyo 152, Japan*

⁽⁵⁾ *Dept. of Applied Physics, Tokyo Univ. of Agriculture and Technology, Tokyo 184, Japan*

⁽⁶⁾ *Department of Physics, University of Tokyo, Tokyo 113, Japan*

⁽⁷⁾ *Department of Physics, Osaka City University, Osaka 558, Japan*

⁽⁸⁾ *Department of Physics, Purdue University, West Lafayette, IN 47907, USA*

⁽⁹⁾ *Institute for Nuclear Study, University of Tokyo, Tokyo 188, Japan*

⁽¹⁰⁾ *The Graduate School of Science and Technology, Kobe University, Kobe 657, Japan*

⁽¹¹⁾ *Faculty of Liberal Arts, Tezukayama Gakuin University, Nara 631, Japan*

*To be published in Phys. Lett. **B**.

†internet address: masako@kekvox.kek.jp.

Abstract

We have studied open charm production in $\gamma\gamma$ collisions with the TOPAZ detector at the TRISTAN e^+e^- collider. In this study, charm quarks were identified by electrons (and positrons) from semi-leptonic decays of charmed hadrons. The data corresponded to an integrated luminosity of 95.3 pb^{-1} at a center-of-mass energy of 58 GeV. The results are presented as the cross sections of inclusive electron production in $\gamma\gamma$ collisions with an anti-tag condition, as well as the subprocess cross sections, which correspond to resolved-photon processes. The latter were measured by using a sub-sample with remnant jets. A comparison with various theoretical predictions based on direct and resolved-photon processes showed that our data prefer that with relatively large gluon contents in a photon at small $x(x \leq 0.1)$, with the next-to-leading order correction, and with a charm-quark mass of 1.3 GeV.

1 Introduction

Recently, several experimental collaborations at PEP/PETRA[1], TRISTAN[2, 3], and LEP[4, 5] have reported that high-transverse momentum(P_T) jet production in (quasi-)real $\gamma\gamma$ collisions requires a new mechanism (resolved-photon process) in addition to the direct photon process $\gamma\gamma \rightarrow q\bar{q}$ (Fig.1-(a)). The resolved-photon processes are such mechanisms in which the quark-gluon contents of photons participate in hard scattering to cause the high- P_T jet production[6-8]. The relevant diagrams are shown in Figs. 1-(b) and (c) for one- and two-resolved-photon processes, respectively.

The analyses of $\gamma\gamma$ collisions at TRISTAN[2] and γp collisions at HERA[9] have provided clear results for the production of remnant jets which are regarded as the evidence of the resolved-photon processes.

These recent data on jet production have provided us with some important information concerning the quark and gluon contents of a photon: they are inconsistent with a model which has very hard gluon distribution (LAC3[10]). In the jet analysis[2], however, the sensitivity of the data was limited to high x values ($x > 0.1$) because of the experimental P_T cut applied in jet reconstruction and a theoretical cut (P_T^{min}) introduced in order to justify the perturbative calculation.

Charm-quark production in $\gamma\gamma$ collisions is a good tool for studying the jet production mechanisms in two-photon processes[11]. The reaction has several advantages over light-quark production. Since the charm-quark mass is (relatively) well defined, the free parameter P_T^{min} is unnecessary. The dominant mechanisms for $c\bar{c}$ production are only the direct and the one-resolved processes(photon-gluon fusion); the contribution from the two-resolved process is small. Charmed-hadron production from the vector-meson-dominance model(VDM: Fig.1-(d))[12] is also expected to be negligible in the TRISTAN

energy region. It should also be emphasized that higher order QCD corrections ($O(\alpha_s)$) are available for both the direct and one-resolved processes[11, 13, 14]. Studies of charm production in $\gamma\gamma$ collisions thus provide a good opportunity to probe the gluon density in the photon.

In this paper we report on a measurement of open charm production in $\gamma\gamma$ collisions under an anti(no)-tag condition. In the PEP/PETRA experiments[15] and in our previous paper[13, 14], charm quarks were identified by detecting $D^{*\pm}$ signals. In this paper, we use electrons and positrons in the final states to tag charm-quark production in two-photon processes (hereafter, electron also implies positron). The inclusive electron method is sensitive to the charm-quark production at relatively low P_T , where the one-resolved process contributes significantly. We can access the small Bjorken- x region down to $x \sim 0.02$, where model dependence is the largest among various parametrizations of the gluon density in the photon[10,16-20]. The same kind of inclusive electron analysis was carried out by the VENUS collaboration[21].

1.1 Cross section and Monte-Carlo simulation

In order to compare the data with theoretical predictions of the direct and the resolved processes, we carried out a Monte-Carlo simulation for each process. The cross section for charm-quark pair production in the two-photon process $e^+e^- \rightarrow e^+e^-c\bar{c}X$ was obtained by applying the equivalent real-photon approximation(EPA) to the nearly on-shell virtual photons emitted by the beam electrons[22]. Under the anti-tag condition imposed on the scattered electrons, the photon flux factor can be written as[7, 20, 23, 24]

$$f_{\gamma/e}(x_\gamma) = \frac{\alpha_{em}}{2\pi x_\gamma} \left(1 + (1 - x_\gamma)^2\right) \ln \frac{P_{max}^2}{P_{min}^2} - \frac{\alpha_{em}}{\pi} \frac{1 - x_\gamma}{x_\gamma}, \quad (1)$$

where

$$P_{min}^2 = m_e^2 \frac{x_\gamma^2}{1 - x_\gamma}. \quad (2)$$

Here, P_{min}^2 is the kinematical minimum of the photon virtuality. P_{max}^2 is given by

$$P_{max}^2 = \min(P_{max,kin}^2, Q^2), \quad (3)$$

where $P_{max,kin}^2 = 2E_{beam}^2(1 - x_\gamma)(1 - \cos \theta_{max})$ is the maximum photon virtuality determined by the experimental anti-tag condition. For the scale Q^2 , we set $Q^2 = m_c^2 + P_T^2$ [20]. In this experiment, the scattering angles of the beam electrons were limited to less than 3.2° if their energies were greater than $0.4 E_{beam}$ (i.e. $\theta_{max} = 3.2^\circ$ for $x_\gamma = E_\gamma/E_{beam} < 0.6$). P_{max}^2 was mainly determined by this experimental anti-tag condition. To check the validity of the approximation, the EPA prediction was compared with the exact matrix element calculation[25] for the direct $e^+e^- \rightarrow e^+e^-c\bar{c}$ process. We found that both predictions agree at a 1% level under this anti-tag condition[20].

For the parton distribution inside the photon, we have tried two typical parametrizations given by Drees-Grassie(DG)[16] and by Levy-Abramowicz-Charchula(LAC1)[10] as working examples. The gluon distribution of LAC1 increases more rapidly than that of DG at x less than 0.1.

For the cross sections of the subprocesses ($\gamma\gamma \rightarrow c\bar{c}$, $\gamma g \rightarrow c\bar{c}$, $gg \rightarrow c\bar{c}$, and $q\bar{q} \rightarrow c\bar{c}$) we used the lowest order formulas including the charm-quark mass. The higher order effects were taken into account by appropriately weighting the P_T distribution of charm quarks[11, 13, 14]. We used the BASES/SPRING program[26] to calculate the cross sections of these processes and to generate events at the parton level. The charm-quark mass(m_c) used in the cross-section calculations was changed in the range 1.3 - 1.5 GeV in order to see the effect of the mass. The threshold was set at $2 \times m_D = 3.74$ GeV for the mass of the $\gamma\gamma$ system and at 2×1.6 GeV for that of the $c\bar{c}$ system. The remnant

jets in the resolved process were generated in the beam direction. The produced partons were hadronized by JETSET 6.3[27]. In this program, the (constituent) charm-quark mass($m_{const.}$) was set to be 1.6 GeV. To ensure energy conservation, we adjusted the momentum of the charm quark in the fragmentation stage as $P_{JETSET}^2 = P_{gen}^2 + m_c^2 - m_{const.}^2$. For the fragmentation of the charm quark, we used the Peterson function, and set the parameter ϵ_c to be 0.07. The generated events were passed through the TOPAZ detector simulator so as to take into account any acceptance and resolution effects.

2 Apparatus and event selection

The data were taken with the TOPAZ detector at the TRISTAN e^+e^- collider. The integrated luminosity was 95.3 pb^{-1} and the average center-of-mass energy was 58.0 GeV. The details of the TOPAZ detector are described in references[28, 29]. In this analysis, we used a time-projection chamber (TPC) for tracking and dE/dx measurements for charged tracks. Plastic scintillation counters(TOF) surrounding the TPC were used for time-of-flight measurements. We detected electromagnetic showers with three kinds of calorimeters: a barrel lead-glass calorimeter (BCL), an end-cap Pb-proportional-wire-counter-sandwich calorimeter (ECL), and a forward bismuth-germanate-crystal calorimeter (FCL), which cover polar angular ranges $|\cos\theta| \leq 0.85$, $0.85 \leq |\cos\theta| \leq 0.98$, and $0.972 \leq |\cos\theta| \leq 0.998$ ($= 3.2^\circ$), respectively. Since the FCL is very close to the beam pipe, the calorimeter is protected from beam-induced background by an extensive shielding system[30].

2.1 Two-photon event selection

Two-photon events were detected mainly by the charged-track trigger. The trigger required at least two charged tracks with $P_T > 0.3 - 0.7 \text{ GeV}$ and an opening angle > 45

- 70 degrees (depending on the beam condition). On the other hand, the neutral energy trigger required that the energy deposit in the BCL had to be greater than $2 \sim 4$ GeV, or that in the ECL had to be greater than 10 GeV. The details concerning the trigger system can be found in reference[31]. The trigger efficiency for charmed events in two-photon processes was estimated with a trigger simulation to be about 93%.

The hadronic events produced by two-photon interactions were selected based on the following criteria:

1. The number of charged tracks with $P_T > 0.15$ GeV and the polar angle $|\cos\theta| < 0.83$ had to be at least 4;
2. The position of the origin of the event(i.e. the event vertex), reconstructed from all tracks, had to be within 1.5 cm in the xy-plane and within ± 2.0 cm along the beam line from the interaction point;
3. The visible energy(E_{vis}) of the event had to satisfy $E_{vis} \leq 30$ GeV, where both the charged tracks in the TPC and the neutral clusters in the BCL were used in the calculation of E_{vis} ;
4. The mass of the system of the observed hadrons(W_{vis}) had to be $W_{vis} \geq 3$ GeV, where the tracks in the TPC and the clusters in the BCL were used; and
5. The energy of the most energetic cluster appearing in the BCL, the ECL, or the FCL had to be less than $0.4E_{beam}$.

Criterion 5 ensures the anti-tag condition, which limits the scattering angles of the beam electrons to less than 3.2° . We call these events an anti-tag sample. Substantial part of which had some activities, though of relatively low energy, in the FCL. Our Monte-Carlo study showed that these activities can be naturally understood by remnant jets

in the resolved-photon processes[2, 32]. In order to more closely study these events, we selected them by adding the following criterion: the energy deposit in the FCL had to be in the range $0.5 \text{ GeV} < E_{vis}^{FCL} < 0.25 E_{beam}$; they are called remnant-jet-tagged events. These selection cuts left 27379 anti-tag and 13508 remnant-jet-tag events.

2.2 Electron selection

Among the selected events, electron-track candidates were searched in the momentum range $0.4 \leq P_T \leq 3 \text{ GeV}$ and the polar angle range $|\cos \theta| \leq 0.77$.

The TOPAZ detector allows three methods for electron identification. The energy loss (dE/dx) information from the TPC enables us to separate electrons from hadrons in the momentum region ($P_T < 3 \text{ GeV}$)[33]. The E/P ratio of the energy(E) measured by the BCL and the momentum(P) measured by the TPC can separate electrons clearly. The TOF was useful to resolve electrons from Kaons and protons in the overlapped region of dE/dx.

Since the largest background source in this analysis was the electrons from the γ -conversions at the material in front of the TPC, we first rejected the dominant part of such electrons by the following methods. We reconstructed secondary vertices (V^0 's) from all combinations of two tracks, and calculated the invariant mass of each V^0 assuming that its daughter particles are electrons. For the V^0 -reconstruction, two kinds of vertices, i.e., non-crossing and crossing cases in the xy-plane (perpendicular to the beam axis) were searched. In the former case, the distances of the two tracks at the minimum distance position in the xy-plane were required to be less than 7 cm in the xy-plane and 3 cm in the z-direction. In the latter case, we chose from the two crossing points that with the shorter z-difference, and required it to be less than 1.5 cm. We then rejected the tracks in the pair if its invariant mass was $\leq 80 \text{ MeV}$ in the former or $\leq 150 \text{ MeV}$ in the latter

cases.

We also required the closest approach of each electron-track candidate to the event vertex in the xy-plane to be $< 0.5\text{-}1.5$ cm depending on P_T .

Among the remaining tracks, electron tracks were searched by combining the information from the E/P ratio, dE/dx , and TOF as follows: (1) Charged tracks in the TPC were extrapolated to the BCL. We then selected, for each TPC track, the BCL cluster which was the closest. The E/P of each of the so-selected TPC-BCL combinations had to satisfy $0.75 \leq E/P \leq 1.25$. (2) The dE/dx was calculated for the electron-track candidate to be used in the subsequent electron counting. The resultant dE/dx was mostly contained in the range $5.5 \leq dE/dx \leq 7.5$ keV/cm. (3) To remove Kaons and protons in the dE/dx overlap region, we used information from the TOF and required the track to have a confidence level(CL) of 0.01 or better for the electron hypothesis.

The performance of electron identification is demonstrated in Fig.2, where various distributions (the closest TPC-BCL distance(Fig.2-(a)), the E/P ratio(Fig.2-(b)), the CL for the electron hypothesis in the TOF(Fig.2-(c)), and the dE/dx (Fig.2-(d))) are shown. Notice that these figures were obtained with the electron candidates selected by all of the cuts but the one on each plotted quantity. Notice in particular that Figs.2-(a) to (c) were made with an dE/dx cut ($5.5 \leq dE/dx \leq 7.5$ keV/cm) which was used only for purpose of displaying. As can be seen from the dE/dx distribution in Fig.2-(d), two peaks corresponding to electrons and pions are clearly separated.

We counted the numbers of electrons in each P_T bin by fitting the dE/dx distributions with double Gaussians bin by bin. The P_T binning was selected so as to approximately equalize the number of entries in each bin. The P_T resolutions were smaller than the bin width. The numbers obtained are plotted (closed circles) in Fig.3. The errors are statistical. The numbers of electron candidates summed over the P_T bins were 214.8 ± 15.4

and 88.0 ± 9.3 for the anti-tag and the remnant-jet-tag samples, respectively.

2.3 Background estimation

These electron candidates included background tracks coming from sources other than charm-quark decays. These background sources were studied in detail.

There remained electrons coming from γ -conversions which escaped from pair reconstruction. They were presumably energy-unbalanced pairs, for each of which the lower P_T track was not reconstructed by the TPC. We estimated the failure rate of the V^0 reconstruction by a Monte-Carlo simulation. The failure rate, $\eta = N_{V^0 \text{ failure}}^{M.C.} / N_{V^0 \text{ reconstructed}}^{M.C.}$, was estimated for each P_T -bin and was typically ~ 0.4 . In the calculation, we included contributions from Dalitz decay ($\pi^0 \rightarrow e^+e^-\gamma$) as well as the conversion electron pairs. In order to estimate the number of remaining background tracks from γ -conversions, we multiplied the number of the reconstructed conversion pairs in the experiment by η in each P_T bin and obtained the cross-hatched histogram in Fig. 3. The γ -conversion and Dalitz decay background mainly occupies the low- P_T region, and comprises 23.8% of the selected electron sample.

The background from the single-photon annihilation ($e^+e^- \rightarrow (\gamma) \rightarrow q\bar{q}$) was estimated by a Monte-Carlo simulation with JETSET 6.3[27]. The parameters of this Monte-Carlo program have been tuned by fitting the TOPAZ single-photon annihilation data[34]. We set the maximum fractional photon energy (k_{max}) to be 0.99 for initial-state radiation. The result is shown in Fig. 3 as the open area of the histogram. The electrons which came from single-photon annihilations had high P_T in general, and were estimated to be 11.8%.

The contributions from the $e^+e^- \rightarrow e^+e^-\tau^+\tau^-$ and $e^+e^- \rightarrow \tau^+\tau^-$ processes were studied by Monte-Carlo simulations which were used in previous four-lepton[25, 35] and

lepton pair production[36] analyses. The result is shown in Fig.3 as the singly-hatched area of the histogram, which corresponds to 12.1% of the selected electron sample. This background has a broad P_T distribution.

As for the $e^+e^- \rightarrow e^+e^-e^+e^-(\gamma)$ process, we checked its contamination experimentally. First, we searched for events consisting of tracks all of which were consistent with the electron hypothesis (using dE/dx). The contamination was only 3.0%. The change of the cut on the charged multiplicity in the event selection from 4 to 5 made only 1.6% difference seen in the electron yield. We took these numbers as being systematic errors in the cross-section evaluation.

The beam-gas background was checked by using off-vertex events. The electron yield in these events was consistent with zero.

These background contributions were subtracted from the data on a bin-by-bin basis in further analysis. In total, $112.3 \pm 15.4(\text{stat.}) \pm 11.9(\text{sys.})(\text{anti-tag})$ and $42.9 \pm 9.3(\text{stat.}) \pm 6.2(\text{sys.})(\text{remnant-jet-tag})$ electrons remained after the background subtraction.

3 Results

3.1 Inclusive electron cross sections

In order to compare the data with the theoretical predictions directly, we carried out acceptance corrections and measured (1) the transverse momentum(P_T) dependence of the inclusive electron cross sections in $\gamma\gamma$ collisions with the anti-tag condition and (2) the subprocess cross sections which corresponds to the resolved-photon processes. As mentioned before, the polar angles of the selected electrons were limited to $|\cos\theta| \leq 0.77$ in order to ensure good detector performance in the electron identification. The acceptance was determined by the Monte-Carlo simulations of the direct and resolved processes. The resultant acceptance increased smoothly from 5% to 12% as the electron-

P_T goes up from 0.4 GeV to 3.0 GeV.

The results are shown in Figs.4-(a) and (b) for the inclusive electron cross section as a function of the electron P_T , and in Fig.5 for the cross sections which correspond to the resolved-photon processes. Both of the results are also summarized in Tables 1 and 2, where the first errors are statistical and the second ones are systematic (as discussed below). The errors in Figs.4-(a), (b), and Fig.5 include both of these errors added in quadrature.

The latter cross sections were obtained by using the subsample of remnant-jet-tagged events. With the Monte-Carlo simulation of the resolved-photon process, the efficiency of the remnant-jets leaving an activity greater than 0.5 GeV in the FCL was evaluated to be $73\pm 2\%$, where the error was obtained by comparing the two cases both with and without an intrinsic P_T in the remnant-jet production. On the other hand, that of the direct process was estimated to be about 7%. This contribution was subtracted in order to obtain the cross section of the resolved-photon process. In spite of an extensive shielding system protecting the FCL from beam-induced background, continuous(random) activities were still observable. These activities were estimated to be 10% from independent event samples(large-angle Bhabha events and random triggered events) and were subtracted.

The inclusive electron cross section integrated over the intervals $0.4 \leq P_T \leq 3.0$ GeV and $|\cos\theta| \leq 0.77$ was measured to be

$$19.3 \pm 2.7 \text{ (stat.)} \pm 2.1 \text{ (sys.) pb,}$$

while that of the subprocess (resolved-photon process) over the same intervals was

$$7.8 \pm 1.7 \text{ (stat.)} \pm 1.1 \text{ (sys.) pb.}$$

3.2 Systematic errors

The systematic uncertainty quoted above resulted from the various sources discussed below.

1. The uncertainty from the background estimation for γ -conversions and Dalitz decays was estimated to be 10 - 18% by changing the cuts on V^0 reconstruction, and by using independent information from the inner tracking device. Since we used the actual number of V^0 's to estimate the background, the statistical error on that number was dominant.
2. The cut dependence was studied by changing the cuts for the event and electron selections by $\pm 10\%$ from the nominal cut values. The uncertainty estimated this way was about 15%.
3. Two fitting methods were applied in order to obtain the number of electrons from the dE/dx distribution in each P_T bin. First, the fitting was carried out by fixing the center value and the resolution to the values obtained from the entire electron sample. In the second method, the fitting was carried out by making these parameters completely free. The two methods gave a difference of about 5%.
4. The uncertainty in the luminosity measurement was 4%.
5. The Monte-Carlo statistics for the acceptance correction and the background estimation for the processes $e^+e^- \rightarrow e^+e^-\tau^+\tau^-$ and $e^+e^- \rightarrow q\bar{q}$ were treated as systematic errors. The total systematic error from the Monte-Carlo statistics was 5%.
6. As described before, we regarded the $e^+e^- \rightarrow e^+e^-e^+e^-$ background as being a systematic error source. The systematic error from this source differed from bin to bin, but was typically about 4%.

7. The uncertainty in the tagging efficiency of the remnant-jet (2%) was included in the error on the sub-process cross section.

The total systematic errors were then obtained to be from 20 to 35%, depending on the value of P_T .

4 Discussions

The predictions of the charm-quark-production cross sections based on the direct and resolved-photon processes are compared with the data in Figs.4-(a) and (b), and the integrated cross sections are summarized in Table 2. The lowest-order(LO) predictions are shown in Fig.4-(a), while Fig.4-(b) shows the higher-order(next-to-leading-order(NLO)) predictions[11, 13, 14]. The NLO corrections increase the cross sections by about 31% for the direct process. The effects of the charm-quark mass are also shown in the two histograms of direct+LAC1 predictions in Figs. 4-(a) and (b) as well as in Table 2. From these figures and the table, it is clear that the direct process(solid histogram) alone falls short of the observed inclusive electron cross section, being consistent with the previous $D^{*\pm}$ analysis[13, 14].

The direct process alone cannot explain the remnant-jet activities, either. The subprocess cross sections obtained from the remnant-jet-tag sample are compared to the predictions from the resolved-photon processes alone in Fig. 5, where the NLO corrections are included in the theoretical predictions. From this figure and Fig. 4, we can conclude that the data agree better with the prediction based on the LAC1 parametrization than that based on the DG parametrization. As mentioned before, this inclusive electron measurement is sensitive to the difference in the parton distributions for the kinematical region of x down to 0.02. The difference in the predictions of LAC1 and DG results mainly from

the difference in the gluon distribution at small x less than 0.1. Our results indicate that the gluon content increases rather rapidly at the small- x region($x < 0.1$).

5 Conclusions

We have studied inclusive electron productions in $\gamma\gamma$ collisions at $\sqrt{s} = 58$ GeV and measured the inclusive electron cross sections, imposing an anti-tag condition. The subprocess cross sections corresponding to resolved-photon processes were also measured separately by using a remnant-jet-tag sample. The results were compared with the predictions of charm-quark production based on the direct and resolved-photon processes. Here, in the predictions, the uncertainties caused by the charm-quark mass and the effect of the next-to-leading order corrections were studied. The direct process alone can explain neither the cross sections nor the remnant-jet activities. The comparison with the predictions of the sum of the direct and resolved-photon processes showed that our data were well explained if the LAC1 parametrization, which has relatively large gluon contents at small x , was taken for the parton distribution in a photon and the NLO corrections were included. On the other hand, the DG parametrization could not explain the data even if the NLO corrections and the effect of the charm-quark mass were taken into account.

Acknowledgement

We appreciate useful discussions with Drs. D. Aurenche, M. Drees, and K. Hagiwara concerning the cross section of the charm-quark production and the importance of anti-tag condition. We thank the TRISTAN accelerator staff for the successful operation of TRISTAN. We also thank all of the engineers and technicians at KEK and the other collaborating institutions: Messers H. Inoue, N. Kimura, K. Shiino, M. Tanaka, K. Tsukada, N. Ujiie, and H. Yamaoka.

References

- [1] PLUTO Collab., Ch. Berger *et. al.*, Z. Phys. **C29** (1985) 499; Z. Phys. **C33** (1987) 351;
TPC/2 γ Collab., H. Aihara *et.al.*, Phys. Rev. **D41** (1990) 2667;
CELLO Collab., H. j. Behrend *et.al.*, Z. Phys. **C51** (1991) 365.
- [2] TOPAZ Collab., H. Hayashii *et.al.*, Phys. Lett. **B314** (1993) 149.
- [3] AMY Collab., R. Tanaka *et.al.*, Phys. Lett. **B277** (1992) 215; B.J. Kim *et.al.*, Phys.Lett. **B325** (1994) 248.
- [4] ALEPH Collab., D. Buskulic *et.al.*, Phys. Lett. **B313** (1993) 509.
- [5] DELPHI Collab., P. Abreu *et.al.*, CERN-preprint, CERN-PPE/94-04.
- [6] M. Drees and R. M. Godbole, Nucl. Phys. **B339** (1990) 355.
- [7] P. Aurenche *et.al.*, KEK-preprint, KEK-93-180.
- [8] S. J. Broadsky, T. A. DeGrand, J. F. Gunion, and J. H. Weis, Phys. Rev. Lett. **41** (1978) 672, and Phys. Rev. **D19** (1979) 1418; G. H. Llewellyn-Smith, Phys. Lett. **79B** (1978) 83; H. Terazawa, J. Phys. Soc. of Japan, **47** (1979) 355; K. Kajantie and R. Raitio, Nucl. Phys. **B159** (1979) 528.
- [9] H1 Collab., T. Ahmed *et.al.*, Phys. Lett. **B297** (1992) 205;
ZEUS Collab., M. Derrick *et.al.*, Phys. Lett. **B297** (1992) 404.
- [10] H. Abramowicz, K. Charchula, and A. Levy, Phys. Lett. **B269** (1991) 458.
- [11] M. Drees, M. Kämer, J. Zunft, and P. M. Zerwas, Phys. Lett. **B306** (1993) 371; J. Smith and W. van. Neerven, Nucl. Phys. **274** (1992) 36.

- [12] J. J. Sakurai and D. Schildknecht, Phys. Lett. **B40** (1979) 121; I. F. Ginzburg and V. G. Selbo, Phys. Lett. **B109** (1982) 231.
- [13] TOPAZ Collab., R. Enomoto et. al., Phys. Rev. **D50** (1994) 1879.
- [14] TOPAZ Collab., R. Enomoto et. al., Phys. Lett. **B328** (1994) 535.
- [15] TASSO Collab., W. Braunschweig *et.al.*, Z. Phys. **C47** (1990) 499;
TPC/ 2γ Collab. M. Alston-Garnjost *et.al.*, Phys. Lett. **B252** (1990) 499.
- [16] M. Drees and K. Grassie, Z. Phys. **C28** (1985) 451.
- [17] M. Glück, E. Reya, and A. Vogt, Phys. Rev. **D46** (1992) 1973.
- [18] P. Aurenche, P. Chiappeta, M. Fontannaz, J. P. Guillet and E. Pilon, Z. Phys. **C56** (1992) 589.
- [19] L. E. Gordon and J. K. Storrow, Z. Phys., **C56** (1992) 307.
- [20] H. Hagiwara, M. Tanaka, I. Watanabe, and T. Izubuchi, KEK-preprint, KEK-93-160.
- [21] VENUS Collab., S. Uehara et. al., Z. Phys. **C63** (1994) 213.
- [22] C. Weizäcker, Z. Phys. **88** (1934) 612; E. J. Williams, Phys. Rev. **45** (1934) 729.
- [23] K. Hagiwara, H. Iwasaki, A. Miyamoto, H. Murayama and D. Zeppenfeld, Nucl. Phys. **B365** (1991) 544.
- [24] S. Frixione, M. L. Mangano, P. Nason, and G. Ridolfi Phys. Lett. **B319** (1993) 339.
- [25] M. Kuroda, Meiji Gakuin University (Tokyo) Research J. 424 (1988)27.
- [26] S. Kawabata, Comp. Phys. Comm., **41** (1986) 127.

- [27] T. Sjöstrand, *Comp. phys. Comm.*, **39** (1986) 347; T.Sjöstrand and M.Bengtsson, *Comp. phys. Comm.*, **43** (1987) 367.
- [28] TPC: T. Kamae *et. al.*, *Nucl. Instrum. Meth.* **A252** (1986) 423; Masking: T. Kishida *et. al.*, *Nucl. Instrum. Meth.* **A254** (1987) 367; BCL: S. Kawabata *et. al.*, *Nucl. Instrum. Meth.* **A270** (1988) 11; ECL: K. Fujii *et. al.*, *Nucl. Instrum. Meth.* **A236** (1985) 55; J. Fujimoto, *et. al.*, *Nucl. Instrum. Meth.* **A256** (1987) 449.
- [29] FCL: H.Hayashii *et. al.*, *Nucl. Instrum. Meth.* **A316** (1992) 202.
- [30] Masking: H. Kichimi *et.al.*, *Nucl. Instrum. Meth.* **A334** (1993) 367.
- [31] Trigger: R. Enomoto *et. al.*, *Nucl. Instrum. Meth.* **A269** (1988) 507; R. Enomoto, K. Tsukada, N. Ujiie and A. Shirahashi, *IEEE Trans. NS.* **Vol. 35, No. 1**, 419 (1988); T. Tsukamoto, M. Yamauchi and R. Enomoto, *Nucl. Instrum. Meth.* **A297** (1990) 148.
- [32] T. Tauchi, KEK-preprint, KEK-94-67, to be appeared in the proceedings of XXIXth Recontres de Moriond “QCD and High Energy Interactions”, Meribel, France, March 19-26, 1994.
- [33] TOPAZ collab., K. Nagai *et. al.*, *Phys. Lett.* **B278** (1992) 506.
- [34] TOPAZ collab., I. Adachi *et. al.*, *Phys. Lett.* **B227** (1989) 495.
- [35] TOPAZ collab., H. Hayashii *et. al.*, *Phys. Lett.* **B279** (1992) 422.
- [36] TOPAZ collab., B. Howell *et. al.*, *Phys. Lett.* **B291** (1992) 206.

Table 1, M. Iwasaki et. al., Physics Letters B.

electron- P_T (GeV)	$d\sigma/dP_T$		
	anti-tag	remnant-jet-tag	no-tag
0.4 - 0.5	$56.1 \pm 17.1 \pm 13.6$	$26.0 \pm 11.4 \pm 7.2$	$71.3 \pm 17.3 \pm 16.4$
0.5 - 0.6	$50.6 \pm 13.8 \pm 10.9$	$20.3 \pm 8.3 \pm 5.2$	$48.7 \pm 11.9 \pm 10.6$
0.6 - 0.8	$20.8 \pm 6.0 \pm 4.8$	$8.0 \pm 3.0 \pm 2.3$	$26.6 \pm 5.9 \pm 5.9$
0.8 - 1.1	$8.2 \pm 2.8 \pm 1.7$	$2.9 \pm 1.7 \pm 1.1$	$12.7 \pm 2.9 \pm 2.2$
1.1 - 1.5	$2.2 \pm 1.3 \pm 1.2$	$1.3 \pm 1.1 \pm 0.8$	$3.8 \pm 1.4 \pm 2.0$
1.5 - 3.0	$0.7 \pm 0.3 \pm 0.3$	$0.2 \pm 0.2 \pm 0.2$	$0.9 \pm 0.3 \pm 0.3$

Table 1: Differential cross sections $d\sigma/dP_T$ ($|\cos\theta| \leq 0.77$)(pb/GeV) of inclusive electron productions shown as functions of the electron- P_T . The cross sections with anti-tag and no-tag conditions, as well as the remnant-jet-tag cross section corresponding to the resolved-photon process are shown in the table, where the cross section under the no-tag condition was obtained from the sample without the anti-tag cut (criterion 5) in section 2.1. This cross section was obtained by using the detection efficiency calculated with the photon-flux factor of eq.(1) with $\theta_{max} = \pi$.

Table 2, M. Iwasaki et. al., Physics Letters B.

		anti-tag				remnant jet-tag			
σ_{data}	(pb)	$19.3 \pm 2.7 \pm 2.1$				$7.8 \pm 1.7 \pm 1.1$			
		LO		NLO		LO		NLO	
charm-quark mass	(GeV)	1.5	1.3	1.5	1.3	1.5	1.3	1.5	1.3
σ_{direct}		5.8	6.7	7.6	8.8	-	-	-	-
σ_{DG}	(pb)	1.7	2.2	2.0	2.5	1.7	2.2	2.0	2.5
σ_{LAC1}		5.0	6.8	6.3	8.3	5.0	6.8	6.3	8.3
$\sigma_{direct+DG}$		7.5	8.9	9.6	11.3	-	-	-	-
$\sigma_{direct+LAC1}$	(pb)	10.8	13.5	13.9	17.1	-	-	-	-

Table 2: Measured inclusive electron cross sections integrated over the P_T region from 0.4 to 3.0 GeV for $|\cos\theta| \leq 0.77$, together with the theoretical predictions based on the direct and resolved-photon processes. The dependence on the charm-quark mass and the effect of the NLO corrections are also shown.

Figure captions

Figure 1: Examples of diagrams contributing to the hadron production in two-photon processes: (a) direct(QPM) process,(b) one-resolved-photon process, (c) two-resolved process, (d) VDM process.

Figure 2: Various distributions for electron candidates: (a) the distance between a TPC track and its closest BCL cluster, (b) E/P, (c) the confidence level (CL) for the TOF, and (d) dE/dx. Each of these distributions was obtained with all the cuts but that on the plotted quantity.

Figure 3: Observed number of electrons as a function of P_T . The closed circles are the experimental data, while the histograms are the background components estimated by various methods described in the text. The cross-hatched area is the background from γ -conversions and π^0 Dalitz decays, the singly-hatched area is from $e^+e^- \rightarrow e^+e^-\tau^+\tau^-$, and the open area from single photon annihilations.

Figure 4: Differential cross section, $d\sigma/dP_T$ ($|\cos\theta| \leq 0.77$)(pb/GeV), of inclusive electron productions plotted against the electron- P_T , where anti-tag condition is imposed. The closed circles are the experimental data, while the histograms are the theoretical predictions of (a) LO and (b) NLO ; the solid lines are the direct only, the dotdashed lines are the direct+DG, the dotted lines are the direct+LAC1 with a charm-quark mass of 1.5GeV, and the dashed lines are the direct+LAC1 with a charm-quark mass of 1.3GeV.

Figure 5: Differential cross section, $d\sigma/dP_T$ ($|\cos\theta| \leq 0.77$)(pb/GeV), of inclusive electron productions as a function of the electron- P_T obtained from the remnant-jet-tagged sample. The closed circles are the experimental data, while the histograms are the theoretical predictions with the NLO corrections; the dotdashed line is DG, the dotted line is LAC1 with a charm-quark mass of 1.5GeV, and the dashed line is LAC1 with a charm-quark mass of 1.3GeV.

Figure 1

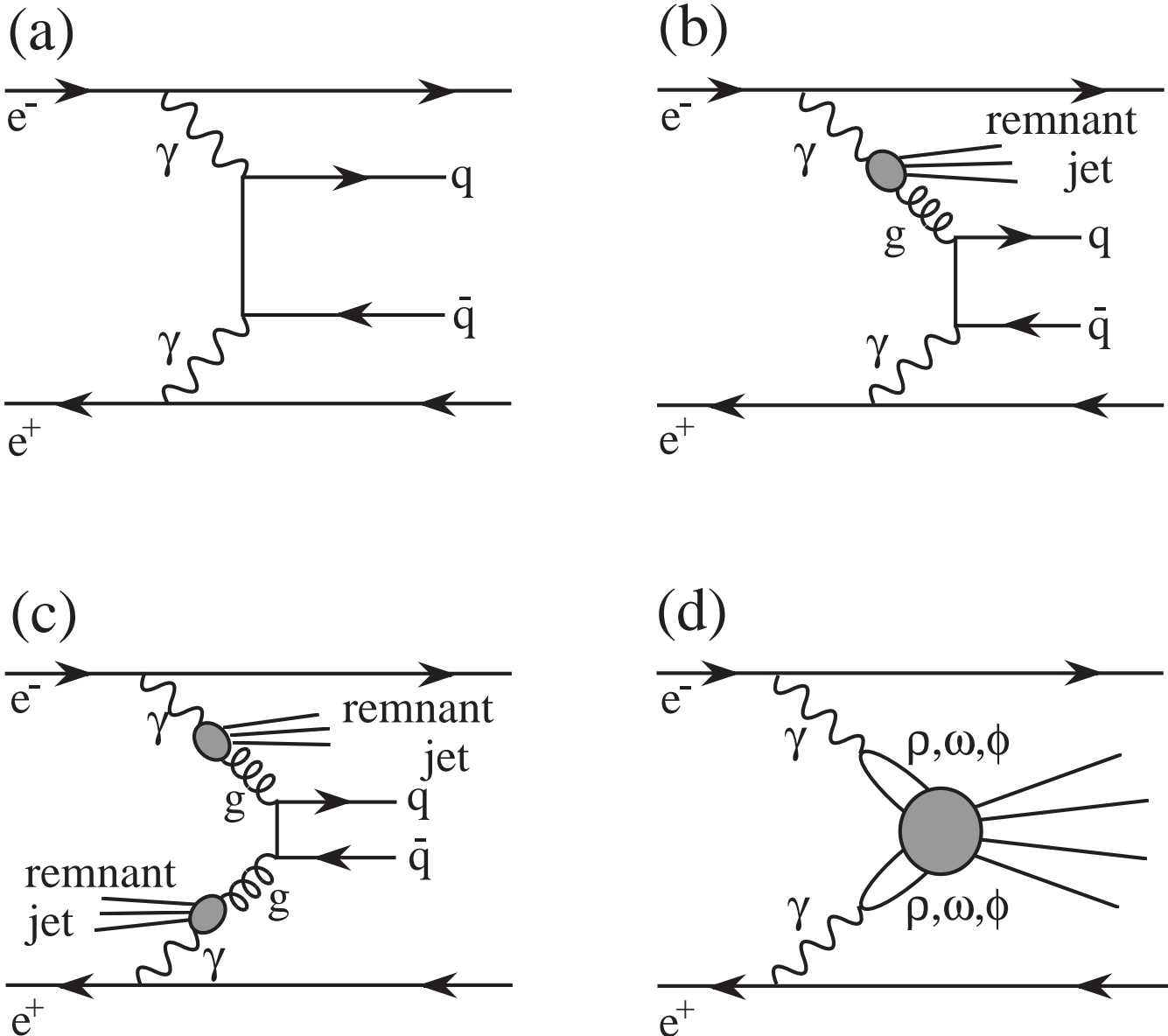


Figure 2

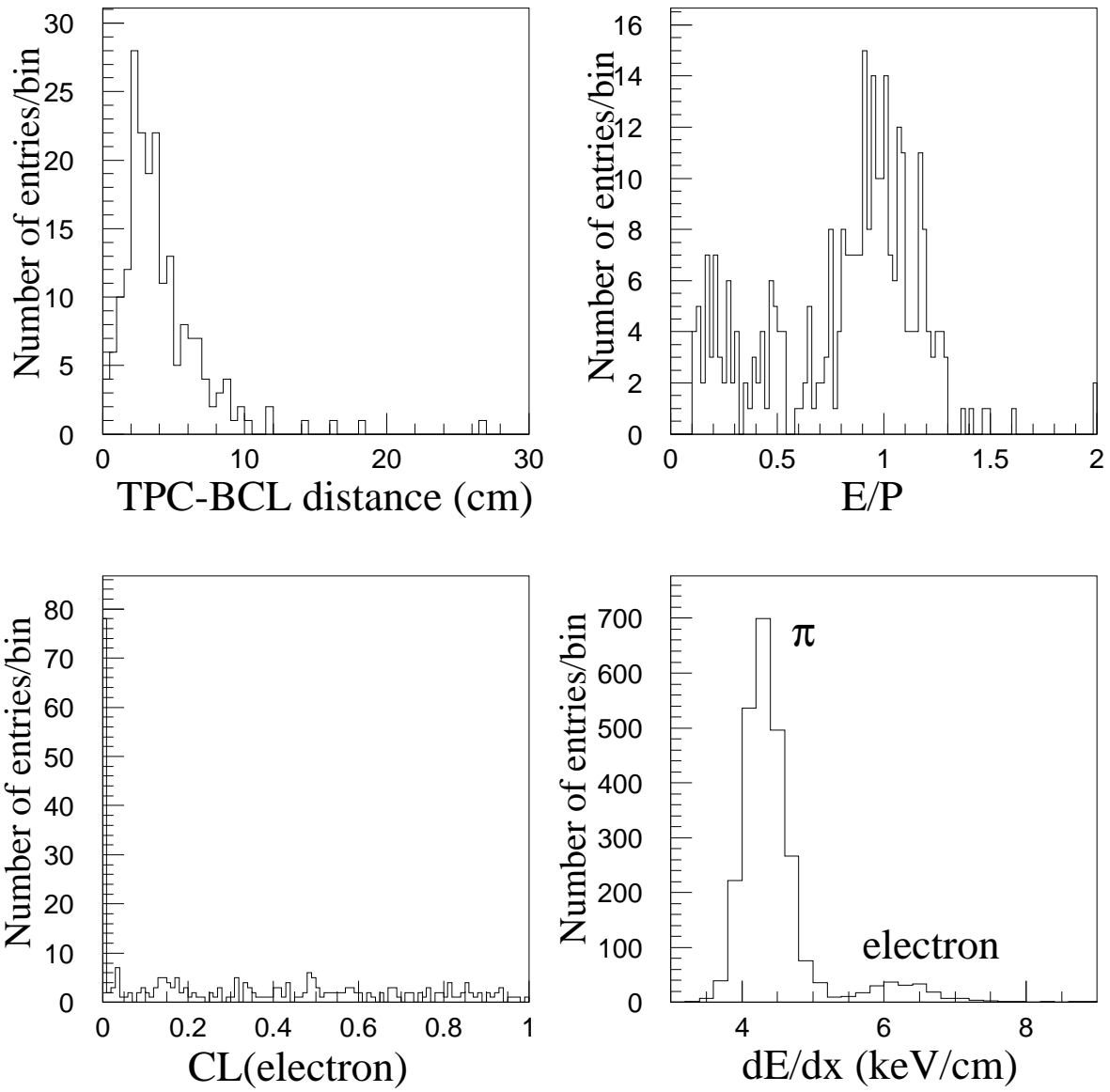


Figure 3

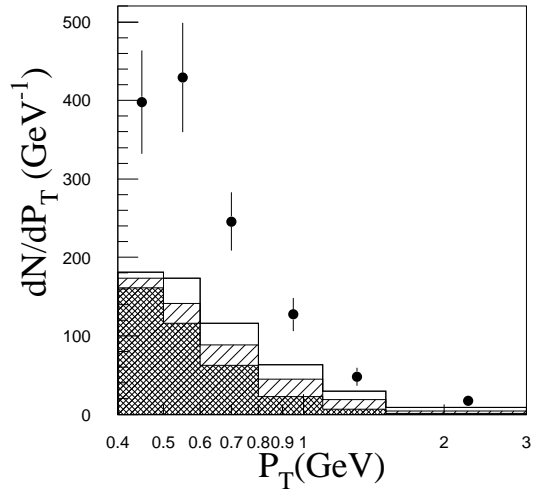


Figure 4

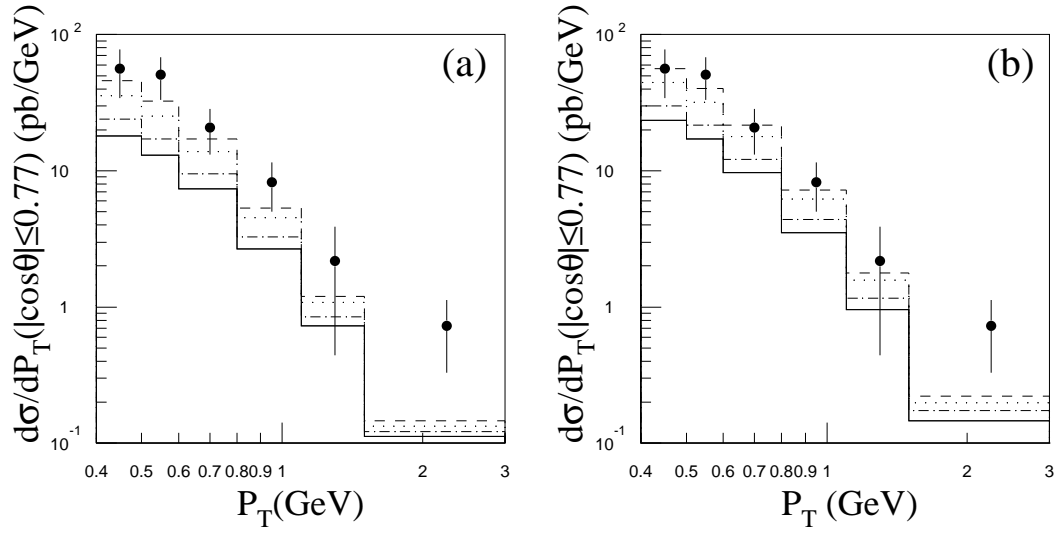


Figure 5

